Optimal Control Applied to Aircraft Flutter Suppression

C. Hwang* and W.S. Pi†
Northrop Corporation, Hawthorne, California

Optimal control techniques were applied to design the reduced order controllers for the purpose of aircraft flutter suppression and load alleviation. Special attention was given to the multiple input, multiple output system to which the classical feedback control theory cannot be conveniently applied. Using the optimal control approach, a number of control laws were designed for an aircraft flutter suppression model. The relative performances of these control laws and previously synthesized control laws were evaluated analytically. In a wind tunnel entry using the flutter suppression model, one of the newly developed control laws was mechanized and successfully demonstrated.

Nomenclature

A,B,C = matrices of the feedback network
$\bar{A}$ = model aerodynamic matrix
$\bar{A}_w$ = aerodynamic matrix due to gust
a,b = constants related to gust spectrum
B = damping matrix
b = characteristic length
F = plant dynamics matrix
G_u, G_w = plant input and gust input matrices
$G_{s,LE}, G_{s,TE}$ = leading edge and trailing edge control surface actuator transfer functions
H, H_D = sensor output matrix and design sensor output matrix
$\bar{H}$ = filter transfer function
$J, \bar{J}$ = performance index and augmented performance index
K = stiffness matrix
$k = \omega b/V$ = reduced frequency
L = gust length
M = mass matrix
N_s, N_0, N_c = number of plant states, observers, controls, respectively
P_0, P_1, P_2 = matrices of aerodynamic coefficients
Q = dynamic pressure
Q_1, Q_2 = design output and control input weighting matrices
R_{u0}, R_v, R_w = noise intensity matrices (all noises are white noises)
$u, u_0, \bar{u}$ = control input and input noise vectors, $\bar{u} = u + u_0$
V = aircraft velocity
v, w = measurement and plant noise (gust) vectors
x_s, x_c = state and control state vectors
y, y_D = output measurement vector and design output measurement vector
Z_0, Z_1 = matrices of gust aerodynamic coefficients
α, β, γ = constants in actuator transfer functions
δ = control surface amplitudes
ζ = a dummy variable
λ_i = eigenvalues
ξ = modal amplitude vector
ρ, ρ_0 = air density and reference air density
ϕ_{w_g} = gust power spectrum
ω = frequency
σ_{w_g} = gust root-mean-square (RMS) value

Submitted May 12, 1982; revision received July 11, 1983.

*Manager, Dynamics and Loads Research, Aircraft Division. Associate Fellow AIAA.
†Senior Technical Specialist, Dynamics and Loads Research, Aircraft Division. Member AIAA.

Introduction

AIRCRAFT active control for load alleviation was initiated and demonstrated in the late sixties.[1] In the past decade, the application was extended to flutter suppression,[2,3] with recent emphasis on fighter aircraft wing/store flutter control.[4,5]

In general, the feedback network for active control may consist of a series of band pass filters and phase shift circuits, organized through cut-and-try or semiempirical procedures, and confirmed by closed loop system analysis. For cases where a single control surface is used for each half wing, a synthesis procedure was applied based on the least square curve-fitting technique to simulate the ideal open loop Nyquist plot of a stable system.[6]

In optimal control, the procedure for determining the linear optimal regulator for a full state system is well known. The full state system is complex in relation to computation and the estimated state variables are sensitive to modelling errors. As a result, reduced order controllers are frequently used.[7,8] In Ref. 9, an adjustment procedure to improve the robustness of the observer based controller to asymptotically achieve the performance of a full state feedback control system was described. The same technique was applied to define active flutter suppression control laws for an aeroelastic wind tunnel model using reduced order controllers.[10] The latter work applied a procedure where the full state optimal feedback and Kalman estimator gain matrices are first determined. For the reduced order controller, the initial values of the design variables are subsets of these matrices. Another application of the linear quadratic Gaussian method for aircraft load alleviation is presented in Ref. 11.

In the semispan wind tunnel test model developed by Northrop, two control surfaces were used to suppress flutter corresponding to various wing/store configurations.[5,12] Using a number of control laws, tests were performed to 70% above the nominal flutter dynamic pressure for a violent flutter case. Evaluation of test results indicates that potential exists to increase the operating dynamic pressure to much higher levels. More recent wind tunnel tests of the same model emphasize the control law mechanization using digital computers, paving the way for future work on adaptive flutter suppression and load alleviation.[13] Since the classical feedback control theory could not be conveniently applied to handle the multiple input, multiple output system (MIMO), it

is considered logical to apply optimal control techniques for flutter suppression and load alleviation. Another motivation of this work is to determine if the previously synthesized single surface control laws can be improved using specific cost functions.

In designing a practical flutter suppression or load alleviation system, it is necessary either to include a large number of natural frequency modes in the analysis, or apply band pass filters to forestall instability due to the adverse excitation of side frequency modes. Using either approach, the dimension of the state variable vector is increased. The reduced order feedback controller can be applied to simplify the analytical procedure and eventually to facilitate the mechanization.

As will be described in the subsequent sections of this paper, the controller design involves the determination of three matrices in the feedback network. Only a portion of the variables forming the matrices are independent, and these are determined by the optimization procedure. Based on previous test experience, the authors have applied a fixed format to part of the feedback network. The fixed format introduces a number of judiciously selected poles in the feedback transfer function. The remaining portion of the controller is determined by the optimization procedure. Once the controller function is determined, the complete closed loop system is examined for stability margins. In other words, the controller is synthesized through the minimization of a performance index under mildly restrictive conditions. During the process, the fictitious noise adjustment procedure for gain and phase margin improvement is applied.

This analysis involves the representation of the gust input as a spectral function. This is accomplished by introducing an additional component in the state variable vector, together with a simplified gust input. Furthermore, the optimal control approach allows the designer to select the specific performance index to be optimized. For instance, the minimization of the aircraft response is of primary interest for the purpose of load alleviation under a given gust condition, while in other cases the magnitudes of control surface activity are critical due to limitations in surface rates, amplitudes, or power requirements.

Using the procedure described in the preceding information, a number of control laws have been developed which are presented in this paper. Also included is a comparison of the predicted performances of the newly synthesized control laws vs those of the previous tested control laws. One of the new optimal control laws was mechanized digitally and tested.[13] The wind tunnel test results are described in the paper.

The Wind Tunnel Test Model

The wind tunnel test model used in this study is a 30% scale half-span model of the YF-17 with a wing tip pylon and under-the-wing pylons. Various flutter sensitive wing/store configurations were established for flutter suppression demonstrations. Two control surfaces were incorporated in the model, one at the wing leading edge, the other at the trailing edge. The key observer signals were supplied by four accelerometers embedded in the wing structure. A sketch of the model is shown in Fig 1. Previous analytical and experimental results acquired from this model are described in Refs. 6 and 12.

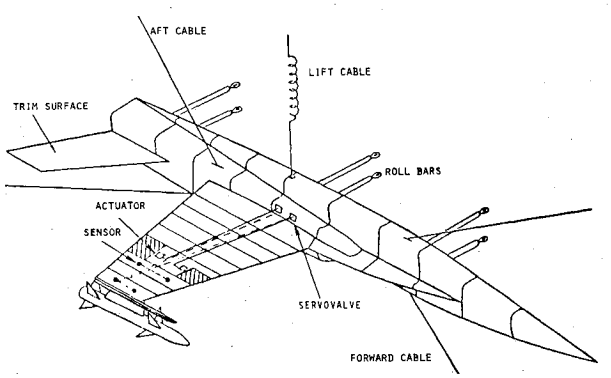

Fig. 1 YF-17 wing/store flutter suppression model, Configuration B.

The State Variable Equation and the Optimal Control Formulation

The state variable equation and the optimal control formulation using reduced order controllers can be found in texts on linear optimal control (e.g., Ref. 7). In order to correlate with the more detailed presentation of a closed loop aircraft system, the general formulation is briefly described as follows. The state variable equation is:

$$\{\dot{x}_s\} = [F]\{x_s\} + [G_u]\{\bar{u}\} + [G_w]\{w\} \tag{1}$$

The corresponding measurement equations are

$$\{y\} = [H]\{x_s\} + \{v\}$$

$$\{y_D\} = [H_D]\{x_s\} \tag{2}$$

For a feedback control system, a control variable vector, x_c, is introduced which is governed by the dynamic equation:

$$\{\dot{x}_c\} = [A]\{x_c\} + [B]\{y\} \tag{3}$$

$$\{\bar{u}\} = [C]\{x_c\} + \{u_0\} \tag{4}$$

A block diagram of the complete system applied to flutter suppression is shown in Fig. 2. Referring to the figure, the dynamics involving the aircraft, its control surfaces, and surface actuators are to be translated into a state variable equation. The objective of optimal control is then to determine the independent elements of matrices A, B, and C, while a performance index (PI) is minimized. The optimal control design procedure is described in Refs. 8 and 10. Readers interested in the detail formulation are referred to these papers.

Aircraft Dynamic Equation

The modal equation representing a flexible aircraft in flight is:

$$M\ddot{\xi} + B\dot{\xi} + K\xi - \frac{\rho}{\rho_0}\frac{V^2}{b^2}\bar{A}(k)\xi = \frac{\rho}{\rho_0}\frac{V}{b}\bar{A}_w(k)w_g \tag{5}$$

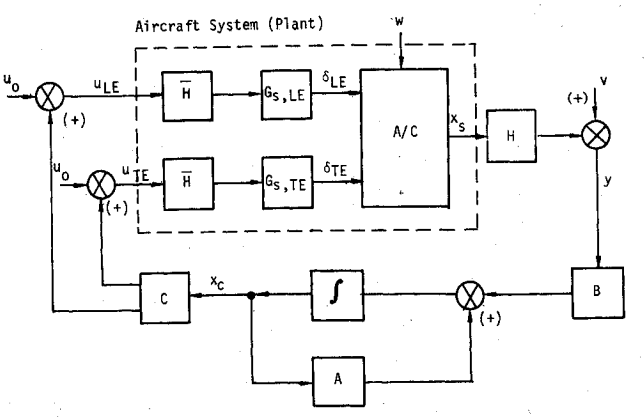

Fig. 2 Block diagram representing the YF-17 model and its flutter suppression system.

Corresponding to each mode ξ, the unsteady aerodynamic force and the gust of Eq. (5) may be approximated as follows:

$$M\ddot{\xi}+B\dot{\xi}+K\xi-\frac{\rho}{\rho_0}\left(\frac{V^2}{b^2}P_0\xi+\frac{V}{b}P_1\dot{\xi}+P_2\ddot{\xi}\right)$$

$$=\frac{\rho}{\rho_0}\frac{1}{V}\left(\frac{V^2}{b^2}Z_0 w_g+\frac{V}{b}Z_1\dot{w}_g\right) \tag{6}$$

The presentation of the unsteady aerodynamic forces by a polynomial of three matrices retains the modal lag information important in aircraft active control. The gust amplitude w_g satisfies the relation:

$$\dot{w}_g+aw_g=bw \tag{7}$$

which corresponds to a gust power spectrum:

$$\phi_{w_g}(\omega)=\frac{b^2}{a^2+\omega^2}R_w \tag{8}$$

The dynamic Eq. (6) can be rewritten in the state variable form:

$$\begin{bmatrix} I & 0 & 0 \\ 0 & C_2 & C_3 \\ 0 & 0 & I \end{bmatrix}\begin{Bmatrix} \dot{\xi} \\ \ddot{\xi} \\ \dot{w}_g \end{Bmatrix}$$

$$=\begin{bmatrix} 0 & I & 0 \\ D_1 & D_2 & D_3 \\ 0 & 0 & a \end{bmatrix}\begin{Bmatrix} \xi \\ \dot{\xi} \\ w_g \end{Bmatrix}+w\begin{Bmatrix} 0 \\ 0 \\ b \end{Bmatrix} \tag{9}$$

where

$$C_2=M-\frac{\rho}{\rho_0}P_2, \qquad C_3=-\frac{\rho}{\rho_0 b}Z_1$$

$$D_1=-K-\frac{\rho V^2}{\rho_0 b^2}P_0, \quad D_2=-B+\frac{\rho V}{\rho_0 b}P_1$$

$$D_3=\frac{\rho V}{\rho_0 b^2}Z_0$$

In the above equation ξ may include control surface motions δ. When δ is included, then elements in the second row of submatrices C_2, C_3, etc., are to be modified as follows: For elements in rows corresponding to the structural modes, the formulation remains unchanged. (These elements include terms representing the unsteady aerodynamic forces due to control surface motion.) For the rows corresponding to the control surface motion, the equilibrium equation is replaced by the dynamic relation between the servo system inputs u [$=Cx_c$, see Eq.(4)] and the surface motions δ. In other words, the rows of elements in the middle band of Eq. (9) are dropped. They are replaced by equations of the actuator dynamics.

Table 1 Control law optimization data ($Q_1=1$, $Q_2=4$, $R_w=100$, $R_v=0.01$)

Control law nos.	R_{u_0}	Initial J	Final J
1	100	8,086	6,027
2	0.4	1,266	752
3	0.25	885	435

$$\delta=\frac{\alpha\gamma}{(s+\alpha)(s^2+\beta s+\gamma)}u=\frac{\gamma}{s^2+\beta s+\gamma}\zeta \tag{10}$$

so that

$$\frac{\alpha}{s+\alpha}u=\zeta \tag{11}$$

With this modification, the aircraft dynamic equation becomes:

$$\begin{bmatrix} I & 0 & 0 & 0 & 0 & 0 \\ 0 & I & 0 & 0 & 0 & 0 \\ 0 & 0 & C_2 & C_{2\delta} & 0 & C_3 \\ 0 & 0 & 0 & I & 0 & 0 \\ 0 & 0 & 0 & 0 & I & 0 \\ 0 & 0 & 0 & 0 & I & 0 \end{bmatrix}\begin{Bmatrix} \dot{\xi} \\ \dot{\delta} \\ \ddot{\xi} \\ \ddot{\delta} \\ \dot{\zeta} \\ \dot{w}_g \end{Bmatrix}$$

$$=\begin{bmatrix} 0 & 0 & I & 0 & 0 & 0 \\ 0 & 0 & 0 & I & 0 & 0 \\ D_1 & D_{1\delta} & D_2 & D_{2\delta} & 0 & D_3 \\ 0 & -\gamma & 0 & -\beta & \gamma & 0 \\ 0 & 0 & 0 & 0 & -\alpha & 0 \\ 0 & 0 & 0 & 0 & 0 & -a \end{bmatrix}\begin{Bmatrix} \xi \\ \delta \\ \dot{\xi} \\ \dot{\delta} \\ \zeta \\ w_g \end{Bmatrix}$$

$$+\begin{bmatrix} 0 & 0 \\ 0 & 0 \\ 0 & 0 \\ 0 & 0 \\ \alpha & 0 \\ 0 & b \end{bmatrix}\begin{Bmatrix} u \\ w \end{Bmatrix} \tag{12}$$

where

$C_{2\delta}$ = inertia forces in other modes due to $\ddot{\delta}$

$D_{1\delta}$ = forces in other modes due to δ

$D_{2\delta}$ = forces in other modes due to $\dot{\delta}$

Equation (12) is further expanded through the insertion of band pass filters $\bar{H}$, which modulate the input signal u (Fig. 2). In our analysis, the filters are represented by a transfer function with a fourth order polynomial (in terms of the Laplace operator s) as the numerator and a seventh order polynomial as the denominator. Based on the above described formulation, the dimension of the state variable is:

$N_s=2\times$ (No. of natural frequency modes)

$+3\times$ (No. of control surfaces)

$+7\times$ (No. of control surfaces with input filters)

$+1$ (Representing the dummy gust variable w_g)

YF-17 Flutter Suppression Control Laws

In our previous wind tunnel entry, the sensors were four accelerometers embedded in the wing structure (see Fig. 1).

Accelerometers y_1, y_2 are located at 81% semi-span and ¼ and ¾ chordwise positions, respectively, and y_3, y_4 are located at 95% semi-span. The feedback network used successfully to suppress flutter featured a series of pseudo-integrators of the form $1/(s+12)$, which convert the accelerometer signals to velocity and displacement signals. The time constant value (0.0833 second) was selected through experimentation. Mixing of the velocity and displacement signals resulted in control signals with proper phasing to suppress flutter. In the present analysis, the four wing accelerometers are retained as the sensor signals ($N_0=4$). Matrix B is either a (4×4) or (8×4) matrix corresponding to either a single surface or two surface control law. The retention of the pseudo-integrators results in an A matrix of the following type:

$$A=\begin{bmatrix} -12 & 0 & 0 & 0 \\ 1 & -12 & 0 & 0 \\ 0 & 0 & -12 & 0 \\ 0 & 0 & 1 & -12 \end{bmatrix} \tag{13}$$

When A is an (8×8) matrix, the (4×4) matrix shown in Eq. (13) is repeated along the diagonal, and null matrices form the off-diagonal submatrices. The B matrix is organized in such a way as to feed the individual observer signals, or their linear combinations, to the odd numbered rows of Eq. (3). It is seen that if A is a fixed (8×8) matrix,

$$B=\begin{bmatrix} 1 & 0 & 0 & 0 \\ 0 & 0 & 0 & 0 \\ 0 & 1 & 0 & 0 \\ 0 & 0 & 0 & 0 \\ 0 & 0 & 1 & 0 \\ 0 & 0 & 0 & 0 \\ 0 & 0 & 0 & 1 \\ 0 & 0 & 0 & 0 \end{bmatrix} \tag{14}$$

then the control signal(s) u can be any linear combination of the integrated y-signals, each of which has proper phasing based on optimal control. In other words, the optimization procedure is reduced to the determination of Matrix C. Typical control laws developed in this manner are based on the following test conditions:

Configuration B (AIM-9E Store at Wing Tip and AIM-7S at W.S. 60.75)

$M=0.8$, $V=420$ fps, $L=1750$ ft

$$\bar{H}=\frac{(s^2+21s+45{,}590)}{(s^2+299s+45{,}590)}\,\frac{s}{(1+0.03s)(1+0.015s)}$$

$$\times\frac{69{,}700}{(s^2+264s+69{,}700)}\,\frac{s}{(s+10)}$$

$$\bar{G}_{S,LE}=\frac{28{,}900}{(s^2+204s+28{,}900)}\,\frac{94}{(s+94)}\quad\text{deg/volt}$$

$$\bar{G}_{S,TE}=\frac{19{,}044}{(s^2+138s+19{,}044)}\,\frac{124}{(s+124)}\quad\text{deg/volt} \tag{15}$$

The $\bar{H}$ filters are bandpass and notch filters, the latter used to prevent local structural resonances. Corresponding to the test conditions described above, the developed control laws are as follows:

Law No. 1, A Leading Edge Surface Law Based on $R_{u_0}=100$

$$u_{LE}=-\frac{1}{s+12}\left[\left(48.8+\frac{436}{s+12}\right)(y_4-y_3)+\left(-55.5+\frac{866}{s+12}\right)(y_3-y_1)\right]$$

Law No. 2, A Two-Surface Law Based on $R_{u_0}=0.4$

$$u_{LE}=-\frac{1}{s+12}\left[\left(34.2+\frac{627}{s+12}\right)(y_4-y_3)+\left(-16.6+\frac{865}{s+12}\right)(y_3-y_1)\right]$$

$$u_{TE}=-\frac{1}{s+12}\left[\left(-9.8+\frac{1.4}{s+12}\right)(y_4-y_3)+\left(-6.4+\frac{1.9}{s+12}\right)(y_3-y_1)\right]$$

Law No. 3, A Two-Surface Control Law Based on $R_{u_0}=0.25$, (Fig. 3)

$$u_{LE}=-\frac{1}{s+12}\left[\left(29.3-\frac{868}{s+12}\right)y_1+\left(1.64-\frac{0.036}{s+12}\right)y_2+\left(-51.33+\frac{241}{s+12}\right)y_3+\left(29+\frac{627}{s+12}\right)y_4\right]$$

$$u_{TE}=-\frac{1}{s+12}\left[\left(-2.65+\frac{0.072}{s+12}\right)y_1+\left(-0.68+\frac{0.2}{s+12}\right)y_2+\left(-2.83+\frac{0.19}{s+12}\right)y_3+\left(-2.05+\frac{0.32}{s+12}\right)y_4\right]$$

For the control laws described above, the performance index J is a quadratic function of the modal responses and the control surface activities. In applying the optimal control technique, the initial and final values of the performance index and the magnitudes of the fictitious noise input R_{u_0} used to reach the final J-values are listed in Table 1. Within an arbitrary but reasonable range of R_{u_0}, the final R_{u_0} value was selected based on the most favorable phase margin.

As a basis of comparison, two control laws developed and tested previously are called Contol Law (NL) and (NLP), respectively. Law (NL) is a leading edge control law, while Law (NLP) uses both control surfaces:

Law (NL)

$$u_{LE}=-\frac{1}{s+12}\left[\left(26.3+\frac{627}{s+12}\right)(y_4-y_3)+\left(-27.3+\frac{869}{s+12}\right)(y_3-y_1)\right]$$

Law (NLP)

$$u_{LE}=-\frac{1}{s+12}\left[\left(26.3+\frac{627}{s+12}\right)(y_4-y_3)+\left(-27.3+\frac{869}{s+12}\right)(y_3-y_1)\right]$$

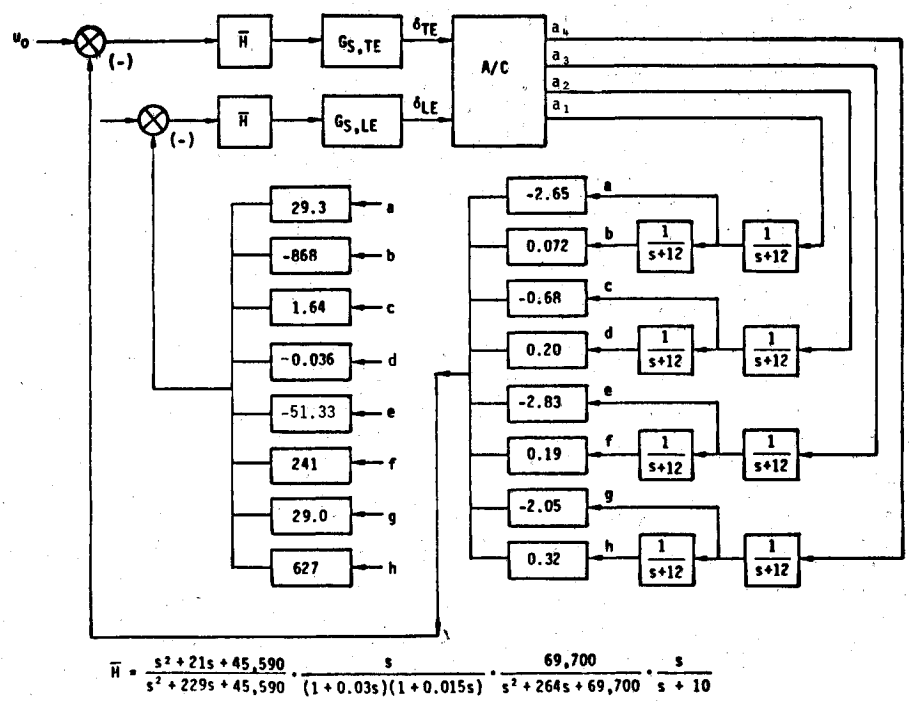

Fig. 3 A two-surface control law (No. 3) for Configuration B.

$$u_{TE} = -\frac{1}{s+12}\left[\left(12.5+\frac{710}{s+12}\right)(y_4-y_3)\right.$$
$$\left.-\left(15+\frac{140}{s+12}\right)(y_3-y_1)\right]$$

In the wind tunnel tests conducted previously, Control Law (*NL*) was tested to 1.70 times the dynamic pressure corresponding to open loop flutter (1.70 Q_f). Extrapolation of the damping trend data indicated a potential to reach 2.40 Q_f before flutter. Control Law (*NLP*) was also tested to 1.70 Q_f. Its predicted flutter dynamic pressure based on extrapolation was 2.04 Q_f. In developing optimized control laws, Law (*NL*) was often used as the starting point. In Fig. 4, the root loci of the key modes which contribute to flutter are plotted for the three optimized control laws. The parameter used in the plots is the dynamic pressure Q. All control laws show a reasonable stability margin up to $Q=160$ psf, or 2.13 Q_f. In Fig. 5, the root loci of the closed loop system corresponding to the previously tested control laws, *NL* and *NLP*, are plotted. An examination of Figs. 4 and 5 data shows that Laws No. 1 and (*NL*), both leading edge control laws, apparently have the same level of stability margin at $Q=160$ psf. On the other hand, Laws No. 2 and 3, both optimized two-surface control laws, feature a superior stability margin at $Q=160$ psf as compared with the previously tested Law (*NLP*).

Figure 6 gives key modal response plots in the form of RMS values vs Q under unit gust for all control laws described above. The responses are computed for the case $R_{u_0}=R_v=0$, i.e., zero control input and measurement noises. It is noted that in the dynamic pressure range under consideration, Control Law (*NL*) is actually superior to the optimized Control Law No. 1 from the response point of view. In contrast, Laws No. 2 and 3 are much superior to the previously tested Law (*NLP*). Figure 7 presents the RMS control surface response data for all control laws under the same gust condition of Fig. 6.

Again the optimized Control Law No. 1 is inferior to Control Law (*NL*) in control surface activity in the sense that the former needs more surface response to deal with identical gust. In evaluating this unexpected and paradoxical situation,

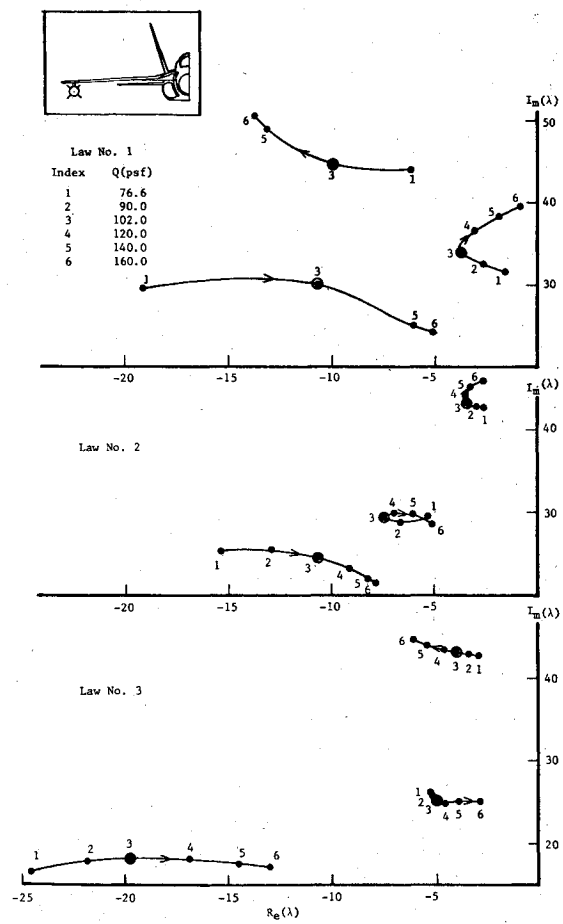

Fig. 4 Root loci of the closed loop system with dynamic pressure as the parameter. The control laws were developed with $Q=102$ psf.

a number of factors come to our attention. First, Law (*NL*) is a very effective control law developed by the Nyquist Curve synthesis procedure.[6] It was used as the starting point to develop Control Law No. 1. During the process, with $R_{u_0}=0$, $R_w=100$, $R_v=0.01$, a control law was developed which had a lower performance index than that of Law (*NL*) under

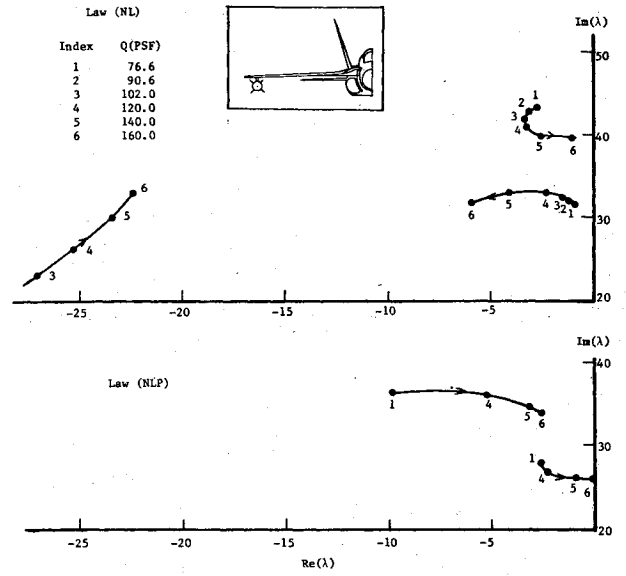

Fig. 5 Root loci of the closed loop system with the dynamic pressure as the parameter. The control laws were used in a previous wind tunnel test.

identical noise conditions. The open loop Nyquist plot of the developed control law is shown in Fig. 8. Because of its unsatisfactory phase margin, a fictitious input noise was introduced. The final control law with satisfactory phase margin was then achieved and named Law No. 1. Law No. 1 corresponds to an input noise level of ($R_{u_0} = 100$). Its open loop Nyquist plot is shown in Fig. 9. Also shown in Fig. 9 is the open loop Nyquist plot of Law (*NL*). It is seen that Law No. 1 does have a somewhat superior phase margin than Law (*NL*) at $Q = 102$ psf. The improvement in phase margin is achieved at the price of higher modal and control surface responses, as illustrated in Figs. 6 and 7.

As far as the two surface control laws are concerned, the control laws developed by the optimal control approach (No. 2 and 3) are superior in overall responses to previously tested Control Law (*NLP*) (see Figs. 5 and 6). Among the two optimized control laws (No. 2 and 3), No. 2 uses three accelerometers as its observers, while No. 3 uses four accelerometers. It is shown that with the additional accelerometer input, Control Law No. 3 is superior to No. 2, with the exception that the former had a trifle higher torsion mode response under gust than No. 2.

Figure 10 shows a root locus type analysis of the closed loop system when Control Law No. 2 was developed. The parameter in this case is the level of the fictitious input noise.

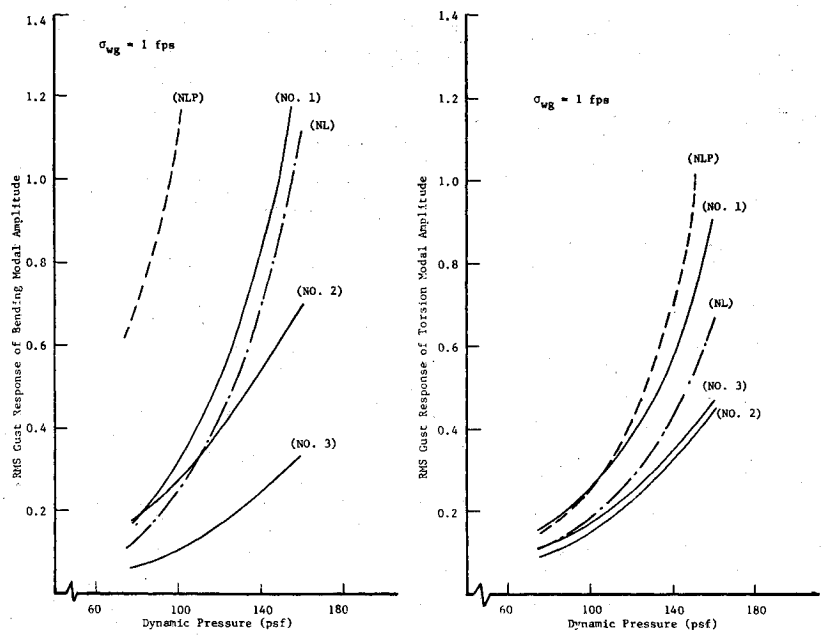

Fig. 6 Comparative performance of the control laws – RMS modal responses under gust. A unit modal amplitude is the one where the maximum normal displacement is 1 in.

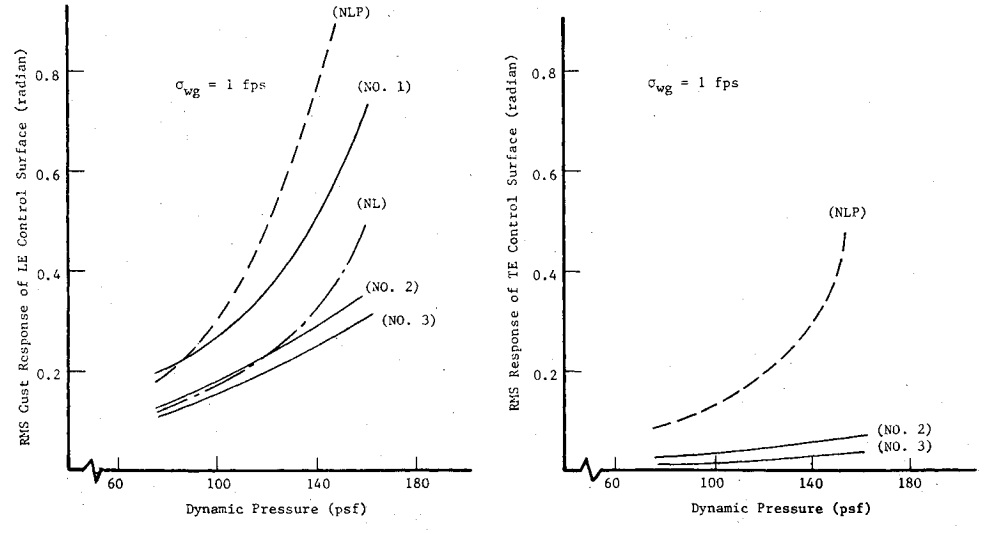

Fig. 7 Comparative performance of the control laws – RMS responses of the control surfaces under gust.

Based on this plot, the finalized Control Law No. 2 was selected using $R_{u_0} = 0.40$, corresponding to Parameter Index No. 4 in the figure.

Wind Tunnel Test Results

Control No. 3 for Configuration *B* of the YF-17 model was mechanized in a digital computer. It was tested at the NASA Langley Research Center's Sixteen-Foot Transonic Dynamics Tunnel at $M = 0.80$ up to a dynamic pressure of 129 psf. In the same program, a previously developed control law (*NL*) was also digitized and tested. The experimental results are evaluated against the analytical performance prediction described in Figs. 6 and 7. For instance, the PSD's of the leading edge surface deflections for Control Laws (*NL*) and No. 3 for $Q \cong 128$ psf are shown in Fig. 11. Integration of the spectral data indicates the leading edge surface activity of Control Law No. 3 is approximately 90% of that of Control Law (*NL*). Integration of the trailing edge surface PSD data (Fig. 12) shows that the T.E. surface RMS value is less than 20% of the L.E. surface RMS value for Control Law No. 3 at $Q \cong 128$ psf. These results are consistent with the analytical prediction of Fig. 7.

The PSD's of the wing bending moment for the two control laws at $Q \cong 128$ psf are processed and presented in Fig. 13. Again the experimental RMS data are consistent with the analytical prediction of Fig. 6, but only in a qualitative sense. Except for the side mode response at approximately 14 Hz, the bending moment response is less for Control Law No. 3 than for Control Law (*NL*). Test data for the torsional moments for the two Control Laws (No. 3 and *NL*) are also consistent with the analytical prediction. For Control Law No. 3, the trailing edge surface activity is substantially less than that of the leading edge surface (see Figs. 11 and 12).

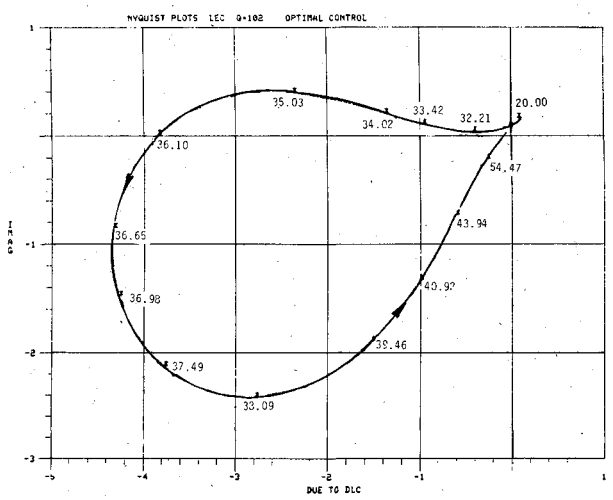

Fig. 8 Open loop Nyquist plot of the flutter suppression system with a preliminary version of Control Law No. 1 engaged, $R_{u_0} = 0$.

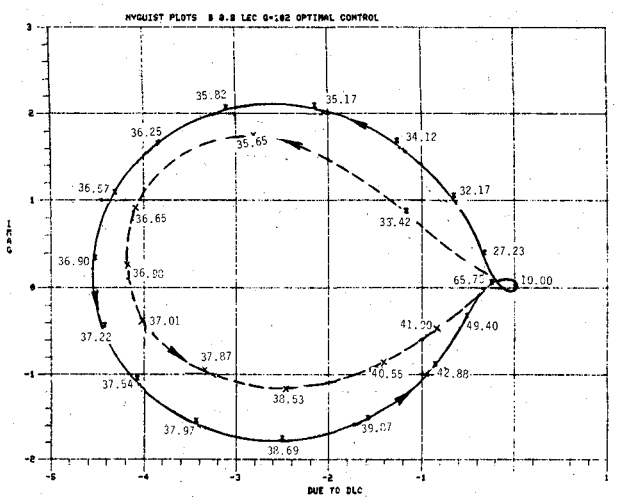

Fig. 9 Open loop Nyquist plots of the flutter suppression system featuring Control Law *NL* (broken curve) and the optimized Control Law No. 1 (solid curve).

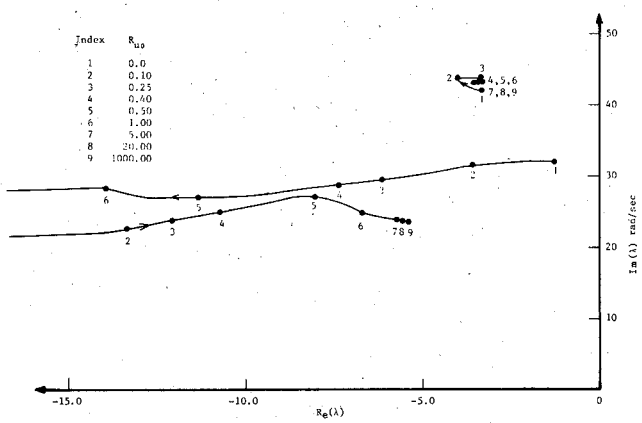

Fig. 10 Root loci of the closed loop system when Control Law No. 2 was developed. The RMS fictitious noise R_{u_0} is the parameter.

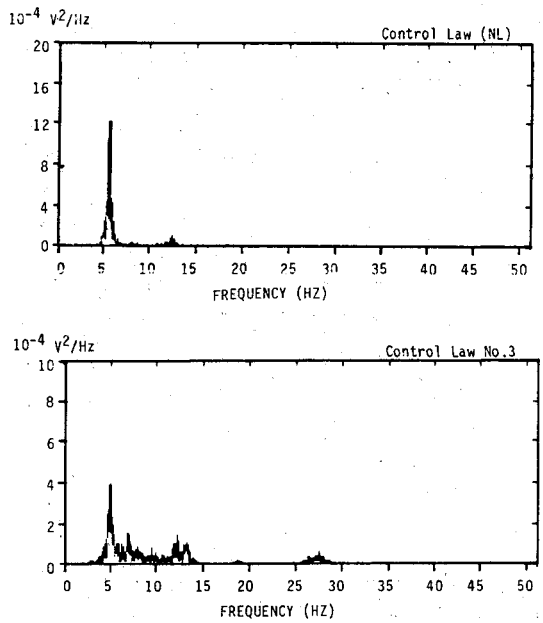

Fig. 11 PSD's of the leading edge deflections for the two control laws at $M = 0.8$ and $Q = 128$ psf. The ordinate conversion factor: 1 V = 7.0 deg.

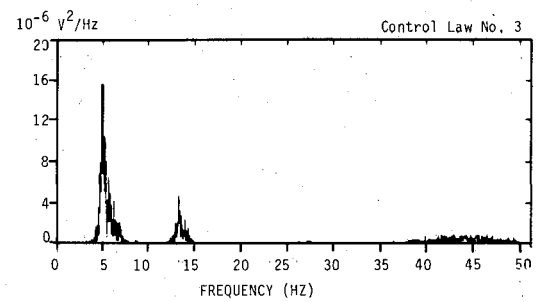

Fig. 12 PSD of the trailing edge surface deflection for Control Law no. 3 at $M = 0.8$ and $Q = 128$ psf. The ordinate conversion factor: 1 V = 7.0 deg.

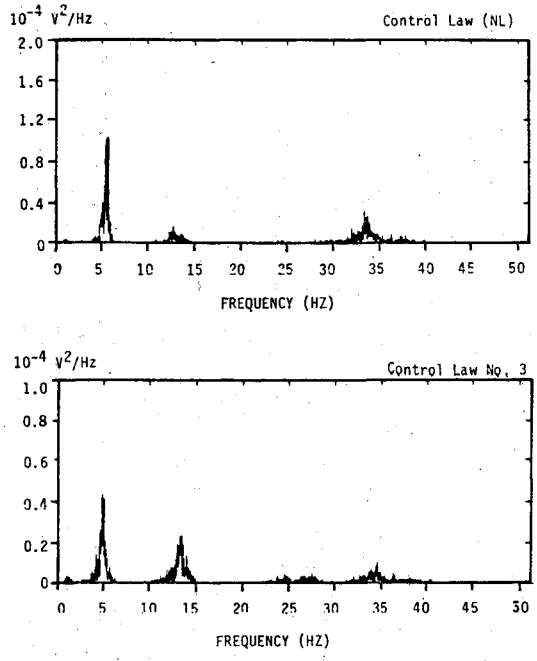

Fig. 13 PSD's of the wing bending moments for two control laws at $M=0.8$ and $Q=128$ psf. The ordinate conversion factor: 1 V = 700,000 in.-lb.

Nevertheless, wind tunnel tests using partial input of this control law demonstrated the significant contribution by the trailing edge surface to control effectiveness.

Strictly speaking, Control Law No. 3 is a two-surface control law. Its performance in the wind tunnel should be compared with that of a two-surface law synthesized by conventional means (such as Law *NLP*). Because of the lack of experimental data, our favorable comparison of Law No. 3 was made against a most effective single-surface law (*NL*). Nevertheless, based on our test experience, it can be stated that optimal Control Law No. 3 is indeed a very successful control law.

Application to Aircraft Load Alleviation

The optimal control approach described in this paper is readily applicable to aircraft load alleviation. Actually, compared to flutter suppression, the requirement in load alleviation is less demanding due to the fact that the initial uncontrolled condition is stable.

For load alleviation, transducers are located at critical locations of the aircraft to sense the structural loads or motion. Proper aerodynamic surfaces are selected for load reduction under gust or other disturbances. Depending on the individual case, either available control surfaces or specially designed and dedicated surfaces may be used. The feedback control network and the actuator power requirement are determined by optimal cotnrol analysis.

Conclusions

In applying optimal control for aircraft systems, the following conclusions are reached:

1) Optimal control is a viable and systematic method for developing flutter suppression control laws. The approach can be applied to deal with aircraft load alleviation problems. We expect increasing emphasis and application of this technique for load alleviation system design in the next generation aircraft.

2) For a reduced order controller, the injection of fictitious input noise is applied to improve phase margins, usually at the price of increasing the overall aircraft responses and control surface activities under gust.

3) The optimal control approach is most effective in developing multiple surface control laws for which no other rational synthesis technique is readily available.

Acknowledgment

The analytical work described in this paper was conducted under a Northrop Independent Research and Development program. The wind tunnel test work was carried out under an AFWAL Contract F33615-80-C-3217 entitled "Test Demonstration of Digital Adaptive Control of Wing/Store Flutter." The Air Force Project Monitor of this contract is Mr. Larry J. Huttsell; the NASA Langley Research Center Test Engineer is Mr. Moses G. Farmer.

References

[1] Morris, P.M. and Bender, M.A., "Aircraft Load Alleviation and Mode Stabilization (LAMS)," AFFDL Rept. TR-68-158, Dec. 1968.

[2] Rogers, K., Hodges, G.E., and Felt, L., "Active Flutter Suppression – A Flight Test Demonstration," *AIAA/ASME/SAE 15th Structures, Structural Dynamics and Materials Conference,* Las Vegas, Nev., April 1974.

[3] Thompson, G.O. and Sevart, F.D., "Wind Tunnel Investigation of Control Configured Vehicle Systems," AGARD Conference Proceedings No. 175, Neuilly Sur Seine, France, July 1975.

[4] Tripplett, W.E., "A Feasibility Study of Active Wing/Store Flutter Control," *Journal of Aircraft,* Vol. 9, June 1972.

[5] Hwang, C., Winther, B.A., Noll, T.E., Farmer, M.G., "Demonstration of Aircraft Wing/Store Flutter Suppression Systems," AGARD Rept. R-668, Neuilly Sur Seine, France, July 1978.

[6] Johnson, E.H., "Flutter Control Law Definition Via Least Square Synthesis," AIAA 21st Structures, Structural Dynamics and Materials Conference, Seattle, Wash., May 1980.

[7] Kwakernaak, H. and Sivan, R., *Linear Optimal Control Systems,* John Wiley and Sons, Inc., New York, 1972, pp. 428-438.

[8] Martin, G.A. and Bryson, A.E., Jr., "Attitude Control of a Flexible Spacecraft," AIAA Paper 78-1281, Aug. 1981.

[9] Doyle J.C. and Stein, G., "Robustness With Observers," *IEEE Transaction on Automatic Control,* Vol. AC-24, Aug. 1979, pp. 607-611.

[10] Mukhopadhyay, V., Newson, J.R., and Abel, I., "A Direct Method for Synthesizing Low-Order Optimal Feedback Control Laws with Application to Flutter Suppression," AIAA Guidance and Control Conference, Danvers, Mass., Aug. 1980.

[11] Gangsaas, D., Ly, U., and Norman, D.C., "Practical Gust Load Alleviation and Flutter Suppression Control Laws Based on a LQG Methodology," AIAA 19th Aerospace Sciences Meeting, St. Louis, Mo., Jan. 1981.

[12] Hwang, C., Johnson, E.H., and Pi, W.S., "Recent Development of the YF-17 Active Flutter Suppression System," AIAA 21st Structures, Structural Dynamics and Materials Conference, Seattle, Wash., May 1980, also *Journal of Aircraft,* Vol. 18, July 1981, pp. 637-645.

[13] Johnson, E.H., Hwang, C., Pi, W.S., Kesler, D.F., and Joshi, D.S., "Test Demonstration of Digital Control of Wing/Store Flutter," AIAA 23rd Structues, Structural Dynamics and Materials Conference, New Orleans, La., May 1982; also *Journal of Guidance, Control, and Dynamics,* Vol. 6, May-June 1983, pp. 176-181.